Complex Formation and Ligand Substitution Reactions of (2-Picolylamine)palladium(II) with Various Biologically Relevant Ligands. Characterization of (2-Picolylamine)(1,1-cyclobutanedicarboxylato)palladium(II)

Tobias Rau, Mohamed Shoukry,[1] and Rudi van Eldik*

Institute for Inorganic Chemistry, University of Erlangen-Nürnberg, Egerlandstrasse 1, 91058 Erlangen, Germany

Received October 1, 1996[⊗]

The influence of a 2-picolylamine (pic) ligand on the reactivity of Pd(II) complexes was investigated by detailed equilibrium and kinetic studies. Reactions of $[Pd(pic)(H_2O)_2]^{2+}$ with chloride, 1,1-cyclobutanedicarboxylic acid ($CBDCAH_2$), inosine (ino), and inosine 5′-monophosphate (5′-IMP) were studied. A significantly higher reactivity for the first reaction step involving the displacement of one coordinated solvent molecule on $[Pd(pic)(H_2O)_2]^{2+}$ was observed for the nucleoside inosine ($k_{10°C} = 25\,400 \pm 200$ M^{-1} s^{-1}) than for the nucleotide 5′-IMP ($k_{10°C} = 7100 \pm 300$ M^{-1} s^{-1}) and for $CBDCAH^-$ ($k_{25°C} = 5380 \pm 70$ M^{-1} s^{-1}; $\Delta H^{\ddagger} = 54 \pm 2$ kJ mol^{-1}; $\Delta S^{\ddagger} = 10 \pm 4$ J K^{-1} mol^{-1}; $\Delta V^{\ddagger} = -0.2 \pm 0.7$ cm^3 mol^{-1}). The results are compared and discussed in reference to data reported for closely related systems in the literature. The molecular structure of [Pd(pic)(CBDCA)] in solution and in the solid state was resolved. $[Pd(pic)(CBDCA)]\cdot 2H_2O$ crystallizes in the space group $P2_1/c$ (monoclinic, $a = 5.659(5)$ Å, $b = 18.320(5)$ Å, $c = 14.027(5)$ Å, $\beta = 97.748(5)°$, $V = 1440.94(14)$ Å^3, $Z = 4$).

Introduction

cis-Diamminedichloroplatinum(II), cisplatin, is one of the most effective agents against cancer of the chest, ovaries, bladder, head, and neck,[2,3] but severe toxicities limit its use.[4,5] In vivo cisplatin binds to DNA to form intrastrand cross-links between two neighboring guanosines, leading to distortion of DNA.[6,7] *cis*-Diammine(1,1-cyclobutanedicarboxylato)platinum-(II), carboplatin,[8,9] the clinically successful second-generation platinum complex, does not exhibit significant nephrotoxicity compared to the first-generation antitumor drug cisplatin. This has been related to the greater pharmacokinetic stability of its 1,1-cyclobutanedicarboxylate (CBDCA) ligand in solution.[10,11] The mode of carboplatin binding to DNA is believed to be the same as that for cisplatin. Ring-opened adducts of carboplatin with L-methionine and guanosine 5′-monophosphate[12] suggest a direct substitution mechanism rather than the involvement of a hydrolyzed species, which is observed in the case of cisplatin. The Pd(II) analogue, $[Pd(NH_3)_2(CBDCA)]$,[13] was shown to be isostructural with carboplatin. Nucleotide adducts of Pd(II) and Pt(II) amine complexes also have the same structures.[14] With 5 orders of magnitude higher reactivities, but similar thermodynamic parameters and structures, analogous Pd(II) complexes are good models for the study of their solution behavior.

Recent work in our laboratories focused on the kinetics and mechanisms of complex formation and ligand substitution reactions of model *cis*-bis(amine)palladium(II) complexes with nucleobases, nucleosides, and nucleotides.[15−20] The goal of these studies was to contribute toward the mechanistic understanding of the interaction of the related anticancer drug cisplatin with DNA and its constituents.[21] Similar studies are presently being performed by others[22,23] on the corresponding Pt(II) complexes. A further objective of our work was to investigate the kinetic tuning of such complexes via steric and electronic effects. In this respect, the introduction of metal−sulfur[24] and metal−carbon bonds[25,26] resulted in a significant labilization of the *trans* position in aqueous solution.

⊗ Abstract published in *Advance ACS Abstracts,* March 1, 1997.

(1) On leave from the Department of Chemistry, University of Cairo, Cairo, Egypt.
(2) Krakoft, I. H. In *Platinum and Other Metal Coordination Compounds in Cancer Chemotherapy: Clinical Application of Platinum Complexes*; Nicolini, M., Ed.; Martinus Nijhoff Publishing: Boston, MA, 1988; p 351.
(3) Loehrer, P. J.; Einhorn, L. H. *Ann. Intern. Med.* **1984**, *100*, 704.
(4) Vermorken, J. B.; Pinedos, H. M. *Neth. J. Med.* **1982**, *25*, 270.
(5) Vonhoff, D. D.; Schilsky, R.; Reichert, C. M. *Cancer Treat. Rep.* **1979**, *63*, 1527.
(6) Takahara, P. M.; Rosenzweig, A. C.; Frederick, C. A.; Lippard, S. J. *Nature* **1995**, *377*, 649.
(7) Reedijk, J. *J. Chem. Soc., Chem. Commun.* **1996**, 801.
(8) Harland, S. J.; Smith, I. E.; Smith, N.; Alison, D. L.; Calvert, A. H. In *Platinum Coordination Complexes in Cancer Chemotherapy*; Hacker, M. P., Douple, E. P., Krakoft, I. H., Eds.; Martinus Nijhoff Publishing: Boston, MA, 1984; p 352.
(9) Egorin, M. J.; van Echo, D. A.; Ohman, E. A.; Whitacre, M. Y.; Forrest, A.; Aisner, J. *Cancer Res.* **1985**, *45*, 6502.
(10) Harland, S. J.; Newell, D. R.; Siddik, Z. H.; Chadwick, R.; Calvert, A. H.; Harrap, K. R. *Cancer Res.* **1984**, *44*, 1693.
(11) Mauldin, S. K.; Husain, I.; Sancar, A.; Chaney, S. G. *Cancer Res.* **1986**, *46*, 2876.
(12) Frey, U.; Ranford, J. D.; Sadler, P. J. *Inorg. Chem.* **1993**, *32*, 1333.
(13) Barnham, K. J.; Djuran, M. I.; Frey, U.; Mazid, M. A.; Sadler, P. J. *J. Chem. Soc., Chem. Commun.* **1994**, 65.
(14) Barnham, K. J.; Bauer, C. J.; Djuran, M. I.; Mazid, M. A.; Rau, T.; Sadler, P. J. *Inorg. Chem.* **1995**, *34*, 2826.
(15) Hohmann, H.; Hellquist, B.; van Eldik, R. *Inorg. Chem.* **1992**, *31*, 345. Hohmann, H.; Hellquist, B.; van Eldik, R. *Inorg. Chem.* **1992**, *31*, 1091.
(16) Shoukry, M.; Hohmann, H.; van Eldik, R. *Inorg. Chim. Acta* **1992**, *198−200*, 187.
(17) Suvachittanont, S.; van Eldik, R. *Inorg. Chem.* **1994**, *33*, 895.
(18) Suvachittanont, S.; Hohmann, H.; van Eldik, R.; Reedijk, J. *Inorg. Chem.* **1993**, *32*, 4544.
(19) Suvachittanont, S.; van Eldik, R. *J. Chem. Soc., Dalton Trans.* **1995**, 2027.
(20) Shoukry, M.; van Eldik, R. *J. Chem. Soc., Dalton Trans.* **1996**, 2673.
(21) Rau, T.; van Eldik. R. In *Metal Ions in Biological Systems*; Sigel, A. Sigel, H., Eds.; Marcel Dekker: New York, 1996; Vol. 32, p 339.
(22) Arpalahti. J. In *Metal Ions in Biological Systems*; Sigel, A., Sigel, H., Eds.; Marcel Dekker: New York, 1996; Vol. 32, p 379.
(23) Mikola, M.; Vihanto, J.; Arpalahti, J. *J. Chem. Soc., Chem. Comm.* **1995**, 1759.
(24) Prinsloo, F. F.; Pienaar, J. J.; van Eldik, R. *J. Chem. Soc., Dalton Trans.* **1995**, 3581.
(25) Schmülling, M.; Ryabov, A. D.; van Eldik, R. *J. Chem. Soc., Dalton Trans.* **1994**, 1257.

S0020-1669(96)01192-5 CCC: $14.00

In this study, we investigated the kinetic and thermodynamic behavior of Pd(II) complexes with a bidentate amine ligand having a heteroaromatic nitrogen base (pyridine) that possesses π-accepting properties, which is believed to be involved in $\pi-\pi$ stacking effects with purine and pyrimidine bases. In this respect, it is very interesting to note that Farrell et al.[27] found a remarkable increase in the cytotoxicity of *trans*-[$Pt(py)_2Cl_2$] complexes in comparison to inactive *trans*-[$Pt(NH_3)_2Cl_2$] by introducing aromatic nitrogen ligands. Our interest in 2-picolylamine as a ligand further results from the fact that it is one of the basic components of a series of new building blocks for biomimetic assemblies recently developed in our laboratories.[28] The use of 2-picolylamine as a ligand is therefore a first step in the application of such assemblies for the development of a new generation of potential antitumor agents. This ligand also enables us to study the electronic labilization induced by the presence of one heteroaromatic ring. Romeo and co-workers[29] recently reported that the rate of DMSO exchange on complexes of the type *cis*-[Pt(N-N)(Me)(DMSO)] increases by 10 orders of magnitude in going from ethylenediamine to dimethylphenanthroline as a diamine chelating ligand. The chelate ring-closure mechanism of 2-picolylamine and similar ligands with *cis*-[$PtPh_2(CO)(SEt_2)$] in dibromethane was also studied by Romeo et al.[30] Here a slow ring closure was observed for the monocoordinated amine.

Equilibrium and kinetic studies on a series of substitution reactions along with the characterization of the complex [Pd(pic)(CBDCA)] enable us to draw a detailed comparison with a series of systems studied previously.[21]

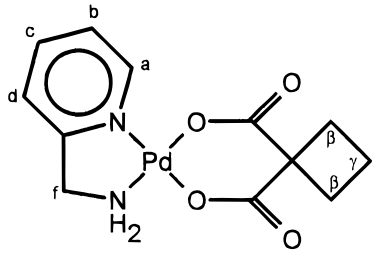

[Pd(pic)(CBDCA)]

Experimental Section

Reagents. $PdCl_2$ was obtained from Degussa, and 1,1-cyclobutanedicarboxylic acid ($CBDCAH_2$) and 2-picolylamine were from Aldrich. For equilibrium and kinetic studies, [Pd(pic)Cl_2] was converted into the diaqua complex by treatment with 2 equiv of $AgClO_4$ as described for [Pd(en)Cl_2].[31] Inosine (ino), inosine 5′-monophosphate (5′-IMP), and guanosine 5′-monophosphate (5′-GMP) were obtained from Sigma and Fluka and used without further purifications. $NaClO_4$ was purchased from Fluka. High-purity water was used to prepare all solutions.

Syntheses. [Pd(pic)Cl_2] was prepared by heating $PdCl_2$ (1.26 g; 7.10 mmol) in 100 mL of H_2O and 7 mL of HCl (37%) to 70 °C for 30 min. After the $[PdCl_4]^{2-}$ solution was cooled to 20 °C, 2-picolylamine (0.735 mL; 7.1 mmol), dissolved in 10 mL of H_2O, was added dropwise to the stirred solution. A yellow precipitate formed, and the mixture was stirred for a further 2 h at 20 °C. After the precipitate was filtered off, it was washed sequentially with H_2O, ethanol, and diethyl ether. Yield: 1.89 g (6.63 mmol; 93%) of yellow powder. Anal. Calcd for $C_6H_8N_2Cl_2Pd$: C, 25.25; H, 2.82; N, 9.81. Found: C, 25.29; H, 2.73; N, 9.68.

[Pd(pic)(CBDCA)]·H_2O was obtained by stirring 310 mg (1.09 mmol) of [Pd(pic)Cl_2] with 356 mg (2.10 mmol) of $AgNO_3$ in 10 mL of H_2O at 20 °C in the dark. After the white AgCl precipitate was filtered off, 146 mg (1.01 mmol) of $CBDCAH_2$, dissolved in 20 mL of H_2O, was added to the yellow filtrate. The pH value was adjusted to 5.0 with NaOH, and the solution was stirred 2 h at 60 °C. After the solution was allowed to stand at 4 °C for 4 days, yellow crystals were obtained, which were isolated by vacuum filtration and washed sequentially with H_2O, ethanol, and diethyl ether. Drying in vacuum gave 188 mg (0.52 mmol; 48%) of fine yellow needles. Anal. Calcd for $C_{12}H_{14}N_2O_4Pd·H_2O$: C, 38.47; H, 4.30; N, 7.48. Found: C, 38.53; H, 4.32; N, 7.38.

Chemical analyses were performed on a Carlo Erba 1106 elemental analyzer.

Spectroscopy. NMR spectra were recorded on a JEOL JNM EX 270 spectrometer at 269.6 MHz for ^1H using TSP (sodium 3-(trimethylsilyl)propionate) as internal standard. NMR samples were prepared in D_2O and measured at 20 °C; complex concentrations were about 10 mM. pH measurements of NMR solutions were carried out directly in the NMR tube at 20 °C with an Aldrich 4 mm combination electrode. DCl, DNO_3, and NaOD solutions were used to adjust the pH. pH readings of D_2O solutions were uncorrected for the deuterium isotope effect and are designated as pH* values. For NMR measurements, the [Pd(pic)Cl_2] complex was converted into the diaqua complex, $[Pd(pic)(D_2O)_2]^{2+}$, because of the low solubility of the former. This was achieved by reacting [Pd(pic)Cl_2] with 1.9 equiv of $AgNO_3$ in D_2O. After the AgCl precipitate was filtered off with the use of a cotton wool plug, the filtrate was directly used for NMR measurements.

IR spectra were recorded on a Mattson Polaris FT IR spectrophotometer using KBr pellets.

Raman spectra of the polycrystalline samples in glass tubes were obtained under ambient conditions using a DILOR XY multichannel spectrometer, equipped with an Ar^+ ion laser, Spectra Physics Stabilite 2014 (514.5 nm, ∼100 mW). UV−vis spectra were recorded on a Shimadzu 2101 spectrophotometer equipped with a thermostated (±0.1 °C) sample cell holder.

pH Titrations. pH titrations were performed on an automatic titrator (Metrohm SM-Titrino 702). The titroprocessor was calibrated with standard buffer solutions prepared according to NBS specifications.[32] The pH electrode used for potentiometric studies was filled with NaCl as electrolyte to prevent precipitation of $KClO_4$.

The acid dissociation constants of $CBDCAH_2$, inosine, inosine 5′-monophosphate, and guanosine 5′-monophosphate were determined by titrating 0.1 mM samples of each with a standard NaOH solution. 5′-IMP and 5′-GMP solutions were prepared in equimolar $HClO_4$ solution in order to protonate the phosphate group. The acid dissociation constants of the coordinated water molecules in $[Pd(pic)(H_2O)_2]^{2+}$ were determined by titrating 0.05 mmol of the complex with NaOH. The formation constants of the complexes were determined by titrating solution mixtures of $[Pd(pic)(H_2O)_2]^{2+}$ (0.05 mmol) and the ligand in concentration ratios of 1:1 for CBDCA and 1:2 (metal:ligand) for the other ligands. The titrating solution mixtures each had a volume of 50 mL, and the titrations were carried out at 25 °C and 0.1 M ($NaClO_4$) ionic strength. A 0.092 M NaOH solution was used as titrant.

The equilibrium constants evaluated from the titration data (summarized in Table 1) are defined by eqs 1 and 2, where M, L, and H

$$p(\mathrm{M}) + q(\mathrm{L}) + r(\mathrm{H}) \rightleftharpoons (\mathrm{M})_p(\mathrm{L})_q(\mathrm{H})_r \quad (1)$$

$$\beta_{pqr} = \frac{[(\mathrm{M})_p(\mathrm{L})_q(\mathrm{H})_r]}{[\mathrm{M}]^p[\mathrm{L}]^q[\mathrm{H}]^r} \quad (2)$$

stand for the $[Pd(pic)(H_2O)_2]^{2+}$ ion, ligand, and proton, respectively. The calculations were performed using the computer program MINIQUAD-75.[33] The concentration distribution diagrams were obtained

(26) Schmülling, M.; Grove, D. M.; van Koten, G.; van Eldik, R.; Veldman, N.; Spek, A. L. *Organometallics* **1996**, *15*, 1384.
(27) Beusichem, M. V.; Farrell, N. *Inorg. Chem.* **1992**, *31*, 634.
(28) Alsfasser, R.; van Eldik. R. *Inorg. Chem.* **1996**, *35*, 628.
(29) Romeo, R.; Scolaro, L. M.; Nastasi, N.; Arena, G. *Inorg. Chem.* **1996**, *35*, 5087.
(30) Romeo, R.; Alibrandi, G.; Arena, G.; Scolaro, L. M.; Plutino, M. R. *Inorg. Chim. Acta* **1995**, *235*, 281.
(31) Mahal, G.; Van Eldik, R. *Inorg. Chem.* **1985**, *24*, 4165.
(32) Bates, R. G. *Determination of pH-Theory and Practice*, 2nd ed.; Wiley Interscience: New York, 1975.
(33) Gans, P.; Asabatini, A.; Vacca, A. *Inorg. Chim. Acta* **1976**, *18*, 237.

Table 1. Equilibrium Constants for CBDCA, Inosine, 5′-IMP, and 5′-GMP Complexes with $[Pd(pic)(H_2O)_2]^{2+}$ at 25 °C and 0.1 M Ionic Strength

system	*p*	*q*	*r*[a]	log *β*[b]
$[Pd(pic)]^{2+}$	1	0	−1	−4.43(1)
	1	0	−2	−13.07(3)
CBDCA	0	1	1	5.46(1)
	0	1	2	8.31(1)
	1	1	0	7.34(3)
inosine	0	1	1	8.65(1)
	1	1	0	7.43(2)
	1	2	0	11.77(4)
5′-IMP	0	1	1	8.99(1)
	0	1	2	15.13(1)
	1	1	0	10.79(6)
	1	1	1	17.02(6)
	1	2	0	14.65(7)
5′-GMP	0	1	1	9.39(1)
	0	1	2	15.55(1)
	1	1	0	10.82(6)
	1	1	1	17.35(7)
	1	2	0	14.46(7)

[a] *p*, *q*, *r* are the stoichiometric coefficients corresponding to $[Pd(pic)]^{2+}$, ligand, and H^+, respectively. [b] Standard deviations are given in parentheses.

with the program SPECIES[34] under the experimental conditions used.

Kinetic Measurements. Kinetic measurements were performed on a Durrum D 110 or an Applied Photophysics stopped-flow instrument coupled to online data acquisition systems. The kinetic traces were evaluated using the KINFIT (OLIS, Bogart, GA) set of programs for the Durrum instrument. Measurements at higher pressures (up to 150 MPa) were performed on a homemade high-pressure stopped-flow instrument.[35] The pH of the solutions was adjusted with $HClO_4$ and NaOH to 3.50, and no buffers were applied. Kinetic measurements, if not otherwise stated, were carried out at a complex concentration of 1×10^{-3} M and a temperature of 25.0 ± 0.1 °C, using a 0.5 M ionic strength, which was adjusted with $NaClO_4$. A higher ionic strength was used for the kinetic runs (0.5 M) than for the pH titrations (0.1 M), since under pseudo-first-order conditions the ionic strength of the reagents partially exceeded 0.1 M. All kinetic measurements were performed under pseudo-first-order conditions; i.e., at least a 10-fold excess of nucleophile was used.

X-ray Crystallography. Crystals of $[Pd(pic)(CBDCA)]\cdot 2H_2O$ suitable for X-ray crystallography were obtained by slow evaporation of an aqueous solution at pH 5. The X-ray crystal structure was determined using a Philips PW1100 diffractometer. All reflections with $I > 2\sigma(I)$ were considered observed and used in the analysis. A total of 3516 reflections were measured, of which 1100 were considered observed. Crystal data and details of the data collection are given in Table 2, and final atomic coordinates and isotropic displacement parameters are given in Table S1 (Supporting Information). For solution and refinement, the programs SHELXS-86 and SHELXL-93 were used.[36] The structure was refined by full-matrix least-squares methods. Selected bond distances and angles are displayed in Table S3 (Supporting Information).

Results and Discussion

^{1}H NMR Spectrum of $[Pd(pic)(D_2O)_2]^{2+}$. The aromatic region of the ^{1}H NMR spectrum of $[Pd(pic)(D_2O)_2]^{2+}$ at pH* 2.88 consists of four resonances for the pyridine protons H(a) to H(d), of which H(a) is shifted upfield by 0.6 ppm due to Pd coordination of pyridine with respect to the free ligand (Table 3). The remaining aromatic protons remain nearly unshifted.

Table 2. Crystallographic Data for $[Pd(pic)(CBDCA)]\cdot 2H_2O$

formula	$C_{12}H_{14}N_2O_4Pd\cdot 2H_2O$
fw	392.68
cryst dimens, mm	0.5 × 0.08 × 0.13
cryst system	monoclinic
space group (No.)	$P2_1/c$ (14)
a, Å	5.659(5)
b, Å	18.320(5)
c, Å	14.027(5)
α, deg	90.000
β, deg	97.748(5)
γ, deg	90.000
V, Å^3	1440.94(14)
Z	4
T, K	293(2)
d_{calc}, g cm^{-3}	1.792
d_{obs}	not determined
μ, cm^{-1}	13.16
index ranges	$-5 \le h \le 5$, $0 \le k \le 19$, $-14 \le l \le 14$
F(000)	776
θ range, deg	2.66−22.01
λ(Mo Kα), Å	0.710 69 (graphite monochromator)
residual electron density, e Å^{-3}	0.18
R_1[a]	0.0776 (for obsd data)
R_2[b]	0.1899 (for obsd data)

[a] $R_1 = \sum(|F_o| - |F_c|)/\sum|F_o|$. [b] $R_2 = [\sum w[(F_o^2 - F_c^2)^2]/\sum[w(F_o^2)^2]]^{1/2}$; $w = 1/[\sigma^2(F_o^2) + (0.1000P)^2 + 0.00P]$ where $P = (\max(F_o^2) + 2(F_c^2))/3$.

The aliphatic CH_2(f) group gives a singlet at 4.28 ppm which is shifted to higher field by about 0.1 ppm with respect to the free ligand. No attempt was made to obtain a spectrum at neutral pH, since deprotonation of a H_2O ligand would lead to dimerization.

^{1}H NMR Spectra of [Pd(pic)(CBDCA)]. The ^{1}H NMR spectrum (see Table 3) of [Pd(pic)(CBDCA)] at pH* 6.80 shows the same aromatic pattern as that of $[Pd(pic)(D_2O)_2]^{2+}$. The H(*β*) and H(*γ*) protons of the cyclobutane group appear as a triplet at 2.96 ppm and a quintet at 1.92 ppm, respectively, corresponding well to literature values of related systems.[12,13,37] Due to coordination to Pd(II) they are shifted downfield by about 0.6 and 0.1 ppm in comparison to those of the free ligand, respectively. If the pH* of the solution is lowered to 2.1, a triplet for the 4H(*β*) arises at 2.54 ppm, which is assigned to the free, mostly diprotonated ligand $CBDCAH_2$. Integration shows that the complex [Pd(pic)(CBDCA)], represented by a triplet at 2.95 ppm, is still the major species present under these conditions. In the aromatic region, peaks for the diaqua complex $[Pd(pic)(D_2O)_2]^{2+}$ are detected in addition to those for [Pd(pic)(CBDCA)]. The coupling constants $^3J(H(\beta),H(\gamma))$ remain at 8 Hz as observed for the free ligand. At neutral pH, the complex remains stable and no ring-opened intermediate or free ligand was detected in the ^{1}H NMR spectra. In comparison to the X-ray structure, where a boat conformation makes each hydrogen atom of the two H(*β*) pairs and one H(*γ*) pair distinguishable, it is not possible to differentiate between them by ^{1}H NMR spectroscopy in solution. Fast flipping of the CBDCA ligand is assumed to account for this.

IR and Raman Spectra. The IR spectra of the complexes $[Pd(pic)Cl_2]$ and $[Pd(pic)(CBDCA)]\cdot H_2O$ exhibit strong NH absorption bands in the range 3100−3230 cm^{-1}. *δ*(NH) bands are observed at 1580−1609 cm^{-1} for the dichloro and at 1595 cm^{-1} for the dicarboxylate complex, respectively. The carboxylate stretching bands ν_a and ν_{as} appear at 1626 and 1379 cm^{-1}, respectively, corresponding to a unidentate coordination

(34) Pettit, L., University of Leeds. Personal communication.
(35) van Eldik. R.; Gaede, W.; Wieland, S.; Kraft, J.; Spitzer, M.; Palmer, D. A. *Rev. Sci. Instrum.*, **1993**, *64*, 1355.
(36) (a) Sheldrick, G. M. SHELXS-86. Institut für Anorganische Chemie, Universität Göttingen, Germany, 1986. (b) Sheldrick, G. M. SHELXL-93: A program for crystal structure refinement. Institut für Anorganische Chemie, Universität Göttingen, Germany, 1993.
(37) Rau, T. Diplomarbeit, University of Dortmund, 1994.

Table 3. ^{1}H NMR Data for 2-Picolylamine and CBDCA Complexes of Pd(II) Obtained in D_2O: Chemical Shifts (ppm) and Coupling Constants (Hz)

		NMR						
	pH*	H(a)	H(b)	H(c)	H(d)	CH_2(f)	H(β)	H(γ)
pic	2.75	8.64(d)	7.61(t)	8.10(t)	7.66(d)	4.41(s)		
		4.4	6.6	7.7	8.8			
	6.81	8.60(d)	7.42(t)	7.93(t)	7.52(d)	4.35(s)		
		4.4	6.6	7.7	8.8			
$CBDCAH_2$[12]	2.00						2.56	2.01
								8.0
$CBDCA^{2-}$ [12]	7.00						2.34	1.82
								8.0
$[Pd(pic)(H_2O)_2]^{2+}$	2.88	7.98(d)	7.47(t)	8.07(t)	7.55(d)	4.28(s)		
		5.9		7.7	7.3			
[Pd(pic)(CBDCA)]	6.80	8.09(d)	7.59(t)	8.03(t)	7.51(d)	4.28(s)	2.96(t)	1.92(q)
		5.9	6.3	7.3	8.1		7.7	8.1
$[Pd(NH_3)_2(CBDCA)]$[13]	2.5						2.96	1.91
[Pd(en)(CBDCA)][37]	6.75						2.95	1.92

mode.[38] Pd−N absorptions are detected at 460 and 438 cm^{-1} (Raman) and 461 cm^{-1} (IR) for $[Pd(pic)Cl_2]$. In the Raman spectrum, the Pd−N bands of $[Pd(pic)(CBDCA)]\cdot H_2O$ appear in the region from 420 to 565 cm^{-1}, where they are intensively overlapped with the Pd−O bands. The Pd−Cl band of $[Pd(pic)Cl_2]$ gives a signal at 326 cm^{-1}.[39] Lattice water of $[Pd(pic)(CBDCA)]\cdot H_2O$ is observed at 3395−3520 cm^{-1} and could not be removed during extensive drying in vacuum.

Equilibrium Studies. The UV−vis spectrum of $[Pd(pic)(H_2O)_2]^{2+}$ exhibits an absorption maximum at 340 nm, which gradually shifts to 355 nm on addition of small amounts of Cl^-. Upon addition of an excess of Cl^-, the maximum shifts to 360 nm according to the complex formation reactions outlined in (3). Values of K_1 were determined by recording spectra of a 1

$$[Pd(pic)(H_2O)_2]^{2+} + Cl^- \overset{K_1}{\rightleftharpoons} [Pd(pic)(H_2O)Cl]^+ + H_2O \quad (3a)$$

$$[Pd(pic)(H_2O)Cl]^+ + Cl^- \overset{K_2}{\rightleftharpoons} [Pd(pic)Cl_2] + H_2O \quad (3b)$$

mM solution of $[Pd(pic)(H_2O)_2]^{2+}$ ($\epsilon = 337$ M^{-1} cm^{-1} at $\lambda =$ 320 nm) in the presence of 0.08−1.6 mM Cl^-. Analysis[25] of the spectra at 320 nm resulted in a K_1 value of 1070 ± 80 M^{-1}. Similarly, by recording the spectra of $[Pd(Pic)(H_2O)Cl]^+$ ($\epsilon =$ 431 M^{-1} cm^{-1} at $\lambda = 390$ nm) in the presence of 2−8 mM Cl^-, we determined a value of 170 ± 12 M^{-1} for K_2. The concentration distribution of the mono- and dichloro complexes is given in Figure 1a. The results are compared in Table 4, with the corresponding data for the closely related ethylenediamine and substituted ethylenediamine complexes.[40] From Table 4 it follows that the K_1 value for the 2-picolylamine complex is significantly smaller and the K_2 value is significantly larger than those for the ethylenediamine complexes. This means about that significantly less of the monoaqua complex is present in solution in the case of the 2-picolylamine complex, since it is converted to either the diaqua or the dichloro form, depending on the chloride concentration in solution.

The acid−base equilibria of $[Pd(pic)(H_2O)_2]^{2+}$ have been characterized by fitting their potentiometric titration data to various acid−base models. The fitted model, according to the aforementioned method of calculation, was found to be consistent with the deprotonation of two coordinated water molecules, as given in (4). The pK_{a3} and pK_{a4} values were found

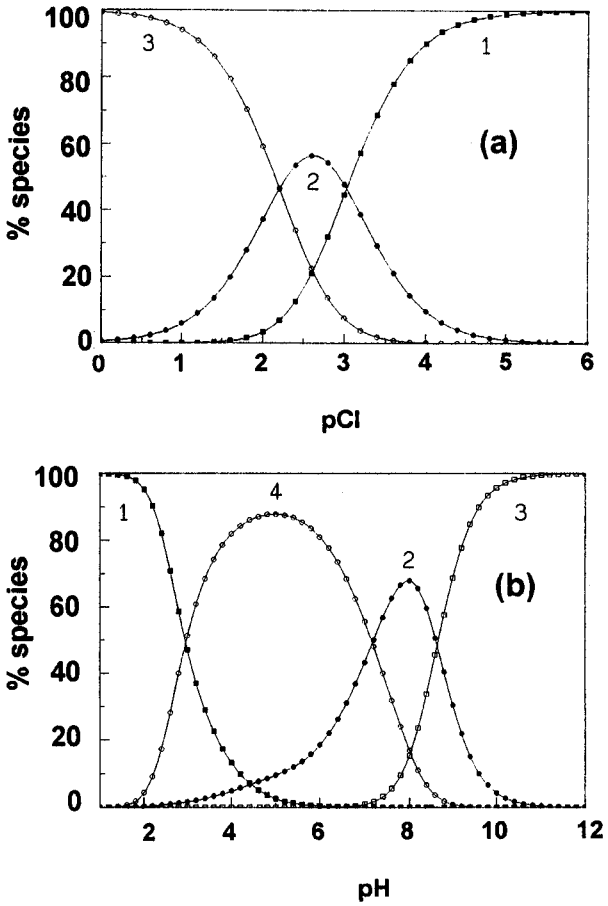

Figure 1. (a) Concentration distributions for various species as a function of pCl in the Pd(pic)−C1 system at pH 4.5: (1) $[M(H_2O)_2]^{2+}$; (2) $[M(H_2O)Cl]^+$; (3) $[M(pic)Cl_2]$. (b) Concentration distribution for various species as a function of pH in the Pd(pic)−CBDCA system: (1) $[M(H_2O)_2]^{2+}$; (2) $[M(OH)]^+$; (3) $[M(OH)_2]$; (4) [M(CBDCA)]. M = $[Pd(pic)]^{2+}$; $T = 25$ °C; $I = 0.1$ M

$$[Pd(pic)(H_2O)_2]^{2+} \overset{K_{a3}}{\rightleftharpoons} [Pd(pic)(H_2O)(OH)]^+ + H^+ \quad (4a)$$

$$[Pd(pic)(H_2O)(OH)]^+ \overset{K_{a4}}{\rightleftharpoons} [Pd(pic)(OH)_2] + H^+ \quad (4b)$$

to be 4.43 and 8.64, respectively. It should be mentioned that the first deprotonation of $[Pd(pic)(H_2O)_2]^{2+}$ is more acidic than that for the $[Pd(R_4en)(H_2O)_2]^{2+}$ systems[40] (see Table 4). This

(38) Nakamoto, N. *Infrared and Raman Spectra of Inorganic and Coordination Compounds*; JohnWiley and Sons: New York, 1986.
(39) Schuhmann, E.; Altman, J.; Karaghiosoff, K.; Beck, W. *Inorg, Chem.* **1995**, *34*, 2316.
(40) Hohmann, H.; Hellquist, B.; van Eldik, R. *Inorg. Chim. Acta* **1991**, *188*, 25.

Table 4. Comparison of Equilibrium Constants for Ethylenediamine, Substituted Ethylenediamine, and 2-Picolylamine Complexes of Pd(II) at 25 °C and 0.1 M Ionic Strength Obtained from Equilibrium Measurements

$$[Pd(N\text{-}N)(H_2O)_2]^{2+} \overset{pK_{a3}}{\rightleftharpoons} [Pd(N\text{-}N)(H_2O)(OH)]^{+} + H^{+}$$

$$[Pd(N\text{-}N)(H_2O)_2]^{2+} + Cl^{-} \overset{K_1}{\rightleftharpoons} [Pd(N\text{-}N)(H_2O)Cl]^{+} + H_2O$$

$$[Pd(N\text{-}N)(H_2O)Cl]^{+} + Cl^{-} \overset{K_2}{\rightleftharpoons} [Pd(N\text{-}N)Cl_2] + H_2O$$

N-N[a]	pK_{a3}, M	K_1, M^{-1}	K_2, M^{-1}
pic	4.4	1070 ± 80	170 ± 12
en	5.6	4000 ± 160	130 ± 14
Me_4en	5.4	3200 ± 500	105 ± 14
Et_4en	5.8	2820 ± 170	52 ± 9

[a] Data for ethylenediamine (en), 1,1,4,4-Me_4en, and 1,1,4,4-Et_4en were taken from ref 40.

can be attributed to the extra stability of the monohydroxo complex, $[Pd(pic)(H_2O)(OH)]^+$, the main species under physiological conditions, which is due to the π-accepting properties of the heteroaromatic nitrogen base. The concentration distribution diagram for the $[Pd(pic)(H_2O)_2]^{2+}$ system is shown in Figure S1 (Supporting Information). It was stated previously that, at a concentration higher than 0.2 mM, more dihydroxo-bridged dimer is present than $[Pd(en)(H_2O)(OH)]^+$.[41] The formation of dimeric species can be neglected by keeping the pH far below the pK_{a3} value. Attempts were made to fit the potentiometric data by assuming the formation of the hydroxo-bridged dimers, but this resulted in very poor fits of the data.

The pK_a's (see Table 1) of ino, 5′-IMP and 5′-GMP agree very well with literature data[42] and also those for CBDCA (pK_a's 2.94 and 5.45; $I = 0.1$ M).[43] The potentiometric equilibrium titration curve of the $[Pd(Pic)(H_2O)_2]^{2+}$−ino system lies significantly lower than the inosine curve (see (Supporting Figure S2 (Supporting Information)). This corresponds to the formation of a complex species through the release of a hydrogen ion, most probably from N1H. The potentiometric data were fitted with models in which hydroxo complex formation was taken into consideration. The accepted model for CBDCA is the 1:1 complex, and there was no evidence for formation of a monoprotonated complex species; i.e., the two carboxylate groups must be ligated to the Pd(II) complex. The titration data for inosine complex formation were fitted by considering the formation of 1:1 and 1:2 complexes. However, the potentiometric data for inosine 5′-monophosphate and guanosine 5′-monophosphate showed the formation of a monoprotonated 1:1 complex, in addition to the formation of 1:1 and 1:2 complexes. The acid dissociation constant of the protonated complex species is given by relation 5,[44] where Nu is the fully deprotonated form

$$pK^{H}_{[M(NuH)]} = \log K^{M}_{[M(NuH)]} - \log K^{M}_{[M(Nu)]} \qquad (5)$$

$$M = [Pd(pic)]^{2+}$$

of 5′-IMP and 5′-GMP. The values of pK^H are 6.23 and 6.53 for 5′-IMP and 5′-GMP, respectively. These values compare favorably with those for the phosphate groups of 5′-IMP and 5′-GMP, amounting to 6.14 and 6.16, respectively. It should be mentioned that the nucleotide complexes are more stable than those of the nucleoside inosine. This may be explained on the basis of different coulombic forces operating between the ions resulting from the negatively charged phosphate groups. Hydrogen bonding between the phosphates and the exocyclic amine is also thought to contribute to the higher stability of the nucleotides over that of the nucleosides.[45]

From a comparison of our findings with those of related studies, it follows that the complexes of the nucleic acid components with $[Pd(pic)(H_2O)_2]^{2+}$ are more stable than those with $[Pd(R_4en)(H_2O)_2]^{2+}$ (R = H, Me, Et).[15,20] The extra stability is a result of the π-accepting properties of the heteroaromatic nitrogen base and the absence of steric hindrance between the alkyl group on R_4en and the incoming ligand.

Species Distribution Plots. In all species distributions (see Figure 1b and Figures S3−S5 (Supporting Information)), the concentration of the formed complex increases with increasing pH, thus making the complex formation more favorable in the physiological pH range, whereas at higher than physiological pH, hydroxo species dominate. Dimerization of hydroxo species can be avoided by using lower complex concentrations and working at lower pH. Since, at pH 3.5 and 1 mM concentrations, the monohydroxo species (see Figure S1 (Supporting Information)) is only present as a minor species, the amount of dimer formed was neglected in the subsequent studies.

In the CBDCA, 5′-IMP, and 5′-GMP systems, the corresponding complexes occur in higher concentration than the hydroxo complexes in the physiological pH range. However, the inosine complex occurs in a lower concentration than the hydroxo complex (see Figure S3 (Supporting Information)). This can be explained on the basis of the fact that the complex formation involving the CBDCA dianion, 5′-IMP and 5′-GMP trianions, and $[Pd(pic)(H_2O)_2]^{2+}$ is electrostatically more favorable than that with inosine. In order to demonstrate the quantitative features observed in the species distribution plots, the speciation diagrams obtained for the Pd(pic)−Cl and −CBDCA systems are shown in Figure 1.

Kinetic Measurements. (a) Reaction of $[Pd(pic)(H_2O)_2]^{2+}$ with CBDCA. The reaction of $[Pd(pic)(H_2O)_2]^{2+}$ with $CBDCAH^-$ (pK_a = 2.85 for $CBDCAH_2$) at pH 3.50 was followed by UV−vis stopped-flow spectroscopy. Repetitive-scan spectra (Figure S6 (Supporting Information)) in which the presence of two reaction steps and the formation of an intermediate were observed were analyzed with the Pro/K software package (Applied Photophysics, Leatherhead KT22 7PB, U.K.). During the reaction, the maximum absorbance shifted from 345 nm for $[Pd(pic)(H_2O)_2]^{2+}$ to 325 nm for [Pd(pic)(CBDCA)]. Kinetic measurements were carried out at 350 nm, where the largest absorption change was observed. Results obtained by measurements at single wavelengths were shown to be identical to those obtained from the repetitive-scan spectra. Two exponential functions were fitted to the absorbance−time trace as shown in Figure 2. The first reaction step shows a linear concentration dependence with $k_{obs} = k_5[CBDCAH^-]$, which represents the substitution of the first coordinated water molecule by $CBDCAH^-$ (see Figure 3 and scheme 6). Under the selected conditions, this reaction step was faster and had larger absorption changes than the second step. No reversibility was observed for this step, as indicated by the absence of a significant intercept in the concentration dependence. The second-order rate constant k_5 derived from the slope of the plot in Figure 3 has a value of 5380 ± 70 M^{-1} s^{-1} at 25 °C. k_5 is assigned to the first nucleophilic substitution step to form the

(41) Martin, R. B. *Platinum, Gold and Other Metal Chemotherapeutic Agents*; Lippard, S. J., Ed.; Advances in Chemistry Series 209; American Chemical Society: Washington, DC, 1983; p 240.
(42) Sigel, H.; Massoud, S. S.; Corfu, N. A. *J. Am. Chem. Soc.* **1994**, *116*, 2958.
(43) *Critical Stability Constants*; Martell, A. E., Smith, R. M., Eds.; Plenum Press: New York, 1977; Vol. 3.
(44) Shoukry, M. *J. Inorg. Biochem.* **1992**, *48*, 271.
(45) Reedijk, J. *Inorg. Chim. Acta* **1992**, *198−200*, 873.

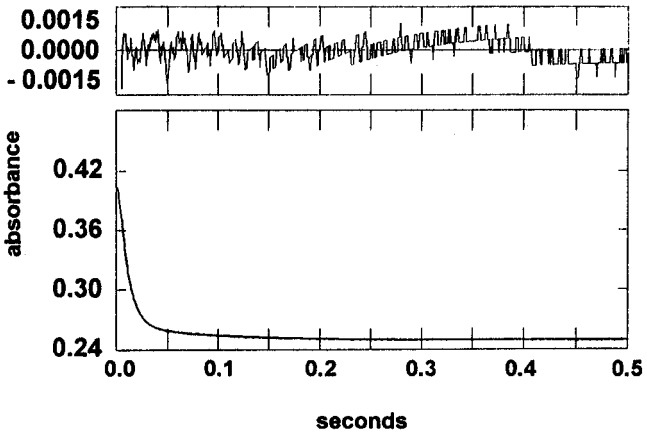

Figure 2. Typical absorbance−time trace for the reaction of $[Pd(pic)(H_2O)_2]^{2+}$ with $CBDCAH^-$ fitted with two exponential functions. The top of the figure shows the absorbance difference between measured and calculated kinetic traces. $[Pd(II)] = 1 \times 10^{-3}$ M; $[CBDCAH^-] = 2 \times 10^{-2}$ M; $I = 0.5$ M; pH 3.50; $\lambda = 350$ nm; $T = 25$ °C.

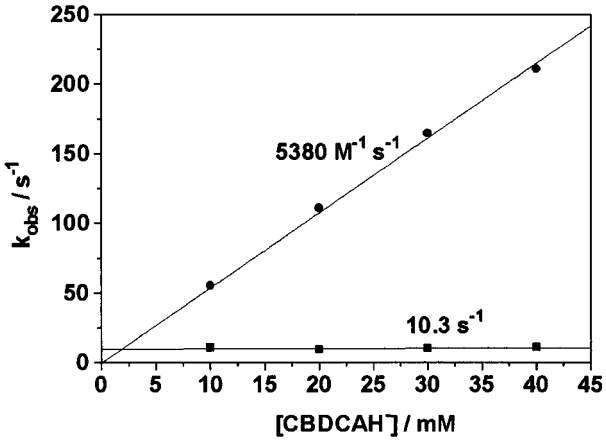

Figure 3. Plot of k_{obs} versus $[CBDCAH^-]$ for both reaction steps outlined in (6). Experimental conditions: $[Pd(II)] = 1.0 \times 10^{-3}$ M; pH 3.50; ionic strength = 0.5 M; $T = 25$ °C.

ring-opened adduct [Pd(pic)(CBDCA-*O*)(H_2O)]. With the release of one proton, which is accompanied by a decrease in the pH value from 3.5 to ca. 3.1 during the reaction, the ring-opened adduct directly reacts further to form the chelated adduct [Pd(pic)(CBDCA-*O*,*O*)]. The pK_a value of the ring-opened adduct is, on the basis of the values for CBDCA, expected to be ≤3 (see further discussion). This reaction step was found to be concentration independent, which is characteristic for a ring-closure reaction (see Figure 3). The rate constant for this process, k_6, has a value of 10.3 ± 0.7 s^{-1} at 25 °C.

$$[Pd(pic)(H_2O)_2]^{2+} + CBDCAH^- \xrightarrow{k_5} [Pd(pic)(CBDCA\text{-}O)(H_2O)] + H_2O + H^+ \quad (6a)$$

$$[Pd(pic)(CBDCA\text{-}O)(H_2O)] \xrightarrow{k_6} [Pd(Pic)(CBDCA\text{-}O,O)] + H_2O \quad (6b)$$

The pH dependence (Figure S7 (Supporting Information)) of the reaction of $[Pd(pic)(H_2O)_2]^{2+}$ with CBDCA shows an increase of the k_{obs} value for the first substitution process from 35 to 175 s^{-1} for pH 2.5 and 4.0, respectively. This increase is mainly attributed to the acid−base equilibria of the CBDCA ligand. With pK_a values of 2.85 and 5.46 for the first and second deprotonation steps, respectively, the monoprotonated form predominates between pH 3.0 and 4.0 whereas, at pH 2.5 and lower, the fully protonated species is the main form in solution, inhibiting the ligand's reactivity. No significant deprotonation of $[Pd(pic)(H_2O)_2]^{2+}$ (pK_{a3} 4.4) occurs in this pH range. At pH 4.0, the concentration of the monohydroxo−monoaqua complex increases to about 30% but is only about 10% at pH 3.5, where a significant interference of the reaction can be excluded.

Table 5. Summary of k_5 and k_6 Along with Activation Parameters for the Reaction of $[Pd(pic)(H_2O)_2]^{2+}$ with $CBDCAH^-$

	k(25 °C)[a]	$\Delta H^{\ddagger}$,[b] kJ mol^{-1}	$\Delta S^{\ddagger}$,[b] J K^{-1} mol^{-1}	$\Delta V^{\ddagger}$,[c] cm^3 mol^{-1}
k_5	5380 ± 70 M^{-1} s^{-1}	54 ± 2	10 ± 4	-0.2 ± 0.7
k_6	10.3 ± 0.7 s^{-1}	60 ± 15	-21 ± 16	

[a] pH 3.50, $I = 0.5$ M. [b] $[Pd(II)] = 1 \times 10^{-3}$ M, $[CBDCAH^-] = 2 \times 10^{-2}$ M, pH 3.50, $I = 0.5$ M. [c] $[Pd(II)] = 5 \times 10^{-4}$ M, $[CBDCAH^-] = 5 \times 10^{-3}$ M, pH 3.50, $I = 0.5$ M.

The effect of temperature on the reactions outlined in (6) was studied at seven different temperatures in the range from 15 to 45 °C, and the results, along with the associated activation parameters, are summarized in Table 5. The activation enthalpies ($\Delta H^{\ddagger}$) obtained from the temperature dependence (Table 5) of 54 ± 2 and 60 ± 1 kJ mol^{-1} for k_5 and k_6, respectively, correspond well with those found for related Pd(II) complexes with substituted amine ligands.[46] For other substitution reactions of $[Pd(H_2O)_4]^{2+}$ with acetic, propionic, and glycolic acids, $\Delta H^{\ddagger}$ values between 52 and 56 kJ mol^{-1} were reported recently,[47] corresponding well to those found for the reaction of $[Pd(pic)(H_2O)_2]^{2+}$ with $CBDCAH^-$ in the present study.

For the activation entropies, $\Delta S^{\ddagger}$, more contrary values have been calculated. The first substitution step gave a $\Delta S^{\ddagger}$ value of 10 ± 4 J K^{-1} mol^{-1}, and for the second step, the ring-closure, a value of -21 ± 16 J K^{-1} mol^{-1} was found. With respect to the large errors usually encountered in the calculation of activation entropies, the values can be regarded as close to zero. Literature reports[46,48] indicate larger negative values for $\Delta S^{\ddagger}$ due to an associative substitution mechanism for Pd(II) complexes. A value close to zero could most probably be explained by an associative interchange mechanism. Further mechanistic information can be drawn from the volume of activation.

Since the first step of the reaction of $[Pd(pic)(H_2O)_2]^{2+}$ with $CBDCAH^-$ at a required 10-fold excess concentration of 1×10^{-2} M is too fast to be measured with the high-pressure stopped-flow instrument, lower concentrations of 5×10^{-4} M for $[Pd(pic)]^{2+}$ and 5×10^{-3} M for $CBDCAH^-$ were selected. Due to the resulting smaller absorption changes and the longer dead time of the high-pressure stopped-flow instrument, only one exponential function could be resolved from the absorbance−time traces. This is mainly ascribed to the first reaction step, since the ring-closure reaction (6b) has negligible absorption changes. Measurements at pressures from 5 to 150 MPa lead to nearly constant k_{obs} values for all pressures within the experimental error limits (see Figure S8 (Supporting Information)). The activation volume ($\Delta V^{\ddagger}$) can be calculated from the slope of a plot of ln k_{obs} vs pressure p. For the reaction of $[Pd(pic)(H_2O)_2]^{2+}$ with $CBDCAH^-$, a value of -0.2 ± 0.7 cm^3 mol^{-1} was found for $\Delta V^{\ddagger}$.

In contrast to reactions of Pd(II) complexes of aliphatic amines with different nucleophiles, usually having significantly negative $\Delta V^{\ddagger}$ values,[48] the substitution reaction of $[Pd(pic)(H_2O)_2]^{2+}$ with $CBDCAH^-$ exhibits an activation volume of

(46) Kotowski, M.; van Eldik, R. In *Inorganic High Pressure Chemistry;* van Eldik, R., Ed.; Elsevier Science Publishers: Amsterdam, 1986; p 219.
(47) Shi, T.; Elding, L. I. *Inorg. Chem.* **1996**, *35*, 735.
(48) van Eldik, R.; Asano, T.; le Noble, W. J. *Chem. Rev.* **1989**, *89*, 549.

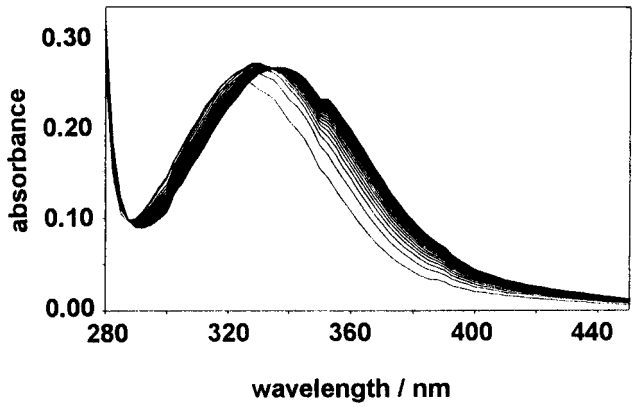

Figure 4. Repetitive-scan spectra for the reaction of [Pd(pic)(CBDCA)] with $HClO_4$. [Pd(pic)(CBDCA)] = 1×10^{-3} M; [$HClO_4$] = 5×10^{-2} M; [$CBDCAH_2$] = 1×10^{-2} M; I = 0.5 M; Δt = 4 ms; T = 25 °C.

approximately zero. Small negative $\Delta V^{\ddagger}$ can indicate a changeover in mechanism from associative (significantly negative $\Delta V^{\ddagger}$ values) to associative interchange (small negative or zero $\Delta V^{\ddagger}$ values). However, other effects can also contribute to the overall value of $\Delta V^{\ddagger}$. The activation volume is mainly composed of two terms, the intrinsic contribution resulting from bond making or breaking and the solvational contribution effected by solvational changes that can result from changes in charge: $\Delta V^{\ddagger} = \Delta V_{intr}^{\ddagger} + \Delta V_{solv}^{\ddagger}$. A large negative $\Delta V_{intr}^{\ddagger}$ resulting from bond formation (associative mechanism) can partly or fully be compensated by a positive influence from $\Delta V_{solv}^{\ddagger}$ due to charge neutralization. In the present case, a 2+ and a 1− species react to produce a 1+ charged product, which, after abstraction of a proton, becomes neutral. A similar result was discussed for the reaction between $[Pd(H_2O)_4]^{2+}$ and glycolic acid, where a small negative value for $\Delta V^{\ddagger}$ was explained in terms of solvational changes.[47] We conclude that, in the present system, intrinsic and solvational contributions almost cancel each other and result in an overall zero $\Delta V^{\ddagger}$ value.

(b) Reaction of [Pd(pic)(CBDCA)] with Acid. Preliminary experiments using ^1H NMR and UV−vis spectroscopy demonstrated that, at a concentration level of 1 mM, the complex [Pd(pic)(CBDCA)] remains stable in solution over a pH range of 3−7. At pH values lower than 3, the coordinated carboxylate groups are protonated and as a result dechelate. At pH ≤1, the CBDCA ligand is quantitatively removed from the metal center. Spectra of the complex [Pd(pic)(CBDCA)]·H_2O, dissolved in H_2O, recorded as a function of pH clearly show a shift in absorbance maximum from 324 to 346 nm on decreasing the pH from 6 to 1, which is characteristic for the aquation of [Pd(pic)(CBDCA)] to $[Pd(pic)(H_2O)_2]^{2+}$. From a plot of the absorbance at 355 nm as a function of pH (see Figure S9 (Supporting Information)), it follows that the overall aquation is characterized by an apparent pK_a value of 2.24. Similar plots of the absorbance maximum and minimum as a function of pH result in pK_a values of 2.15 and 2.13, respectively.

In order to study the acid hydrolysis reaction, [Pd(pic)(CBDCA)]·H_2O was dissolved in H_2O at pH 7 and reacted with an excess of $HClO_4$. Figure 4 shows repetitive-scan spectra at one representative acid concentration recorded during this reaction. The first step (fast reaction) leads to the ring-opened intermediate (λ_{max} = 327 nm) which reacts further (slow reaction) to form the diaqua complex (λ_{max} = 340 nm) and $CBDCAH_2$. From an analysis with the Pro/K software package, the spectrum of the intermediate could also be calculated. At 350 nm, both steps could be analyzed as a function of the proton concentration. A plot of k_{obs} versus [H^+] for both reaction steps (see Figure 5a) indicates a linear dependence on [H^+] with a

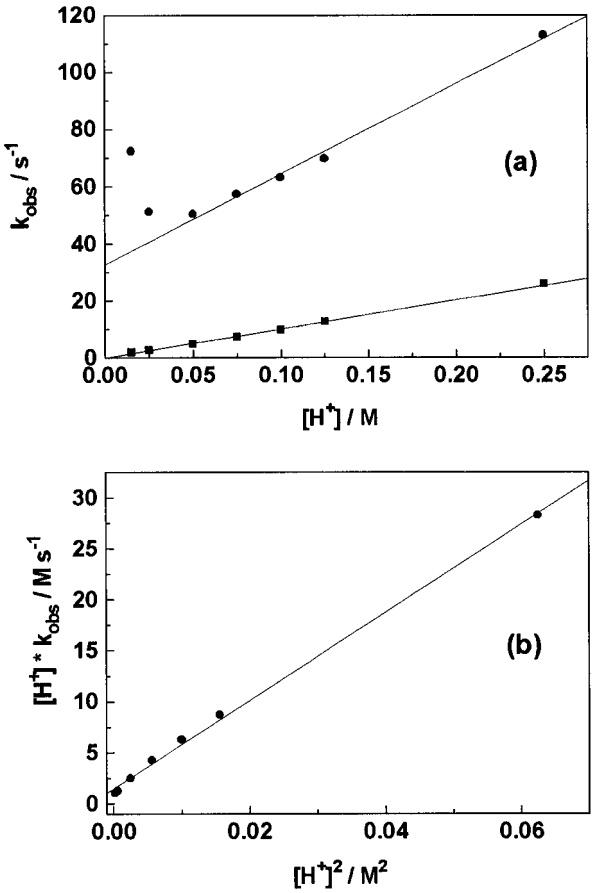

Figure 5. Kinetic plots for the reaction of [Pd(pic)(CBDCA)] with $HClO_4$. Experimental conditions: [Pd(pic)(CBDCA)] = 1×10^{-3} M; λ = 350 nm; ionic strength = 0.5 M; T = 25 °C. (a) k_{obs} versus [H^+]: ●, first reaction step (only values at [H^+] ≥ 0.10 M are used in the data fit); ■, second reaction step (all values shown). (b) [H^+]k_{obs} versus [H^+]^2 (all data for only the first reaction step are displayed).

significant intercept for the first reaction step at [H^+] ≥0.1 M and a linear dependence with no significant intercept over the whole pH range for the second reaction step. The latter trend indicates that the aquation of the ring-opened complex is acid-catalyzed and not reversible. The ring-opening reaction itself is a reversible process, and data at [H^+] < 0.1 M clearly deviate from the linear dependence observed at higher concentrations. Under these conditions, the overall absorbance change decreases with decreasing [H^+], indicating that the reverse ring-closure reaction is favored under such conditions and must account for the increase in k_{obs} with decreasing [H^+]. These data can be explained in terms of the mechanism outlined in (7), which

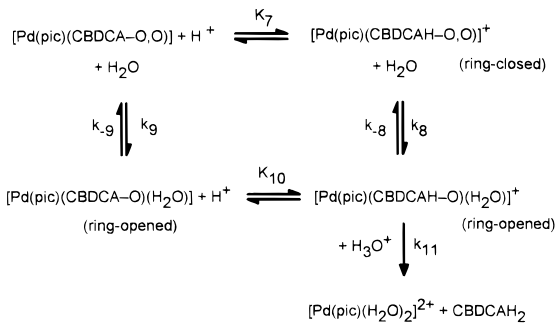

consists of a spontaneous and acid-catalyzed ring-opening process, coupled with the reverse ring-closure process, for the first reaction step. The rate law for this reaction scheme is given in (8), which can be simplified to (9) on the basis of the

$$k_{obs} = \frac{k_8K_7[H^+] + k_9}{1 + K_7[H^+]} + \frac{k_{-8}K_{10}[H^+] + k_{-9}}{1 + K_{10}[H^+]} \quad (8)$$

$$k_{obs} = k_8K_7[H^+] + k_{-9}/K_{10}[H^+] \quad (9)$$

following assumptions. $k_8K_7[H^+] \gg k_9$; acid-catalyzed ring-opening is more efficient than the spontaneous reaction as demonstrated by the pH dependence of the process. $1 + K_7[H^+] \approx 1$; the ring-closed species is fully chelated, which means that protonation of coordinated CBDCA will be thermodynamically unfavorable, although it is required for the acid-catalyzed ring-opening reaction. Large values of K_7 would also lead to a saturation of k_{obs} at high $[H^+]$. It is therefore reasonable to assume that K_7 is indeed very small, such that $1 + K_7[H^+] \approx 1$. $k_{-9} \gg k_{-8}K_{10}[H^+]$; this assumption is based on the argument that ring-closure of the unprotonated ring-opened adduct [Pd(pic)(CBDCA-*O*)(H_2O)] is expected to be much faster than that of the protonated ring-opened adduct. $1 + K_{10}[H^+] \approx K_{10}[H^+]$; the p$K_a$ value of the protonated ring-opened CBDCA ligand is expected to be very close to that of $CBDCAH_2$, from which it follows that $1 + K_{10}[H^+] \approx K_{10}[H^+]$. The apparent p$K_a$ value of 2.2 determined above is indeed very close to that of $CBDCAH_2$ (pK_a 2.85; from Table 1). The difference between the pK_a values is attributed to the 2+ charged Pd complex having a stronger electronic influence than a proton. It follows that these approximations are very reasonable, since ring opening is an acid-catalyzed process, ring-closure is an inverse acid-dependent process, and K_{10} is expected to be ≥100 on the basis of the observed pH dependence. According to eq 9, the data for the ring-opening process should fit eq 10, for which the

$$k_{obs}[H^+] = k_8K_7[H^+]^2 + k_{-9}/K_{10} \quad (10)$$

validity is shown in Figure 5b. It follows from this plot that $k_8K_7 = 431 \pm 9$ M^{-1} s^{-1} and $k_{-9}/K_{10} = 1.5 \pm 0.2$ M s^{-1} at 25 °C.

The subsequent reaction is also an acid-catalyzed process, for which $k_{obs} = k_{11}[H^+]$. The plot of the data in Figure 5a results in $k_{11} = 101 \pm 1$ M^{-1} s^{-1}. This reaction yields the diaqua complex and free ligand, and the absence of a significant intercept indicates the irreversibility of the process under the selected conditions. Deprotonation of $CBDCAH_2$ will naturally lead to the reverse anation reaction studied above. On addition of 5 times the free $CBDCAH_2$ concentration to the reaction mixture, no significant influence on the observed rate constants was found, since the reverse reaction does not occur under such acidic conditions.

(c) Reaction of [Pd(pic)(H_2O)$_2$]$^{2+}$ with Chloride. The anation of [Pd(pic)(H_2O)$_2$]$^{2+}$ by chloride proceeds in two steps as outlined in (3). Under the selected conditions the first step is too fast to be measured by conventional stopped-flow techniques. The rate constant k_{obs} for this step has values >500 s^{-1}. For the second anation step, a linear dependence of k_{obs} on the chloride concentration with a nonzero intercept was found (see Figure S10 (Supporting Information)). This can be expressed by the two-term rate law[49]

$$k_{obs} = k_a + k_b[Cl^-] \quad (11)$$

where k_b represents the concentration-dependent anation reaction with the rate constant k_2. The concentration-independent term k_a represents contributions from the back-reaction k_{-2} and possible side reactions. A rate constant of 1860 ± 30 M^{-1} s^{-1} for k_2 was derived from the slope of the concentration dependence, and a rate constant k_{-2} for the back-reaction of 21 ± 2 s^{-1} was obtained from the intercept. An equilibrium constant of 89 ± 11 M^{-1} for K_2 was calculated from these kinetic data, which is lower than the value of $K_2 = 170 \pm 12$ M^{-1} obtained from the equilibrium studies (see Figure 1). A similar discrepancy was reported for [Pd(en)Cl_2] previously.[49] Here it was stated that the kinetically determined equilibrium constant of 86 ± 2 M^{-1} for the anation step of [Pd(en)Cl(H_2O)]$^+$ also did not comply with that estimated from equilibrium studies having a value of 130 ± 5 M^{-1}. This difference was attributed to the fact that the kinetic intercept represented not only the reverse reaction but also parallel reaction steps, with the result that the intercept was too large and the overall equilibrium constant became too small.[49]

(d) Reaction of [Pd(pic)(H_2O)$_2$]$^{2+}$ with Inosine and 5′-Inosine Monophosphate. The UV−vis spectra for the reaction of [Pd(pic)(H_2O)$_2$]$^{2+}$ with ino and 5′-IMP showed a decrease in absorbance of the [Pd(pic)(H_2O)$_2$]$^{2+}$ band at 345 nm accompanied by an increase at 305 nm. The reactions were followed at 305 nm on a stopped-flow instrument at 10 °C, since they were too fast to be measured at room temperature. During the reaction, the pH remained constant within the range of ±0.05 unit. From the kinetic time traces, two exponential functions could be resolved. The faster reaction step with the larger absorption change was attributed to the substitution of the first coordinated H_2O by ino or 5′-IMP (see scheme 12). From the

$$[Pd(pic)(H_2O)_2]^{2+} + nu^{x-} \underset{k_{-12}}{\overset{k_{12}}{\rightleftharpoons}} [Pd(pic)(nu)(H_2O)]^{(2-x)+} + H_2O \quad (12a)$$

$$[Pd(pic)(nu)(H_2O)]^{(2-x)+} + nu^{x-} \underset{k_{-13}}{\overset{k_{13}}{\rightleftharpoons}} [Pd(pic)(nu)_2]^{(2-2x)+} + H_2O \quad (12b)$$

nu = ino ($x = 0$) or 5′-IMP ($x = 1$)

linear concentration dependences, k_{12} values of 25 400 ± 200 and 7100 ± 300 M^{-1} s^{-1} (see Table 6) were calculated for the first substitution reaction with ino and 5′-IMP, respectively, with the result that ino is reacting about 3−4 times faster than 5′-IMP. The values correspond well to those published for the reaction of [Pd(dien)(H_2O)]$^{2+}$ with nucleic acid components (k_{an} = 26 100 ± 40 M^{-1} s^{-1} for ino; the rate constants for 5′-IMP were also reported to be much smaller than those for ino).[50] It was proposed that the observed step was a secondary process following a fast primary process that involved rapid coordination of the phosphate group. In the case of [Pd(pic)(H_2O)$_2$]$^{2+}$, this is also thought to be the reason for the larger rate constants found for ino than for 5′-IMP. From the concentration dependences (see Figure S11 (Supporting Information)), it is revealed that for the first reaction step a larger intercept resulting in a k_{-12} value of 58 ± 9 s^{-1} is observed for 5′-IMP in comparison to that for ino, for which no significant intercept (20 ± 18 s^{-1}) can be detected. Different results have been found for reactions with [Pt(NH_3)$_2$(H_2O)$_2$]$^{2+}$,[51] where nucleotides exhibit larger rates than nucleosides.

For both nucleophiles, the second reaction step exhibited no dependence on the concentration of the nucleophile, and values of 7.3 ± 0.7 and 32 ± 2 s^{-1} were found for ino and 5′-IMP, respectively, which is rather unusual for such substitution processes. The difference between the equilibrium constants

(49) Hohmann, H.; van Eldik, R. *Inorg. Chim. Acta* **1990**, *174*, 87.
(50) Breet, E. L. J.; van Eldik, R. *Inorg. Chem.* **1987**, *26*, 2517.
(51) Eapen, S.; Green, M.; Ismail, I. M. *J. Inorg. Biochem.* **1985**, *24*, 233.

Table 6. Summary of Rate Constants for the Reactions of Several $[Pd(amine)(H_2O)_2]^{2+}$ Complexes with Inosine and Inosine 5′-Monophosphate

	5′-IMP		ino	
	k_{12}, M^{-1} s^{-1} k_{-12}, s^{-1}	k_{13}, M^{-1} s^{-1} k_{-13}, s^{-1}	k_{12}, M^{-1} s^{-1} k_{-12}, s^{-1}	k_{13}, M^{-1} s^{-1} k_{-13}, s^{-1}
$[Pd(en)(H_2O)_2]^{2+}$		14 200 ± 260[c]	13 600 ± 220[d]	933 ± 63[d]
25 °C; $I = 0.1$ M[15]	*a*	≈0	≈0	8.7 ± 2.3
$Pd(Me_4en)(H_2O)_2]^{2+}$	38 500 ± 1000[c]	265 ± 1[c]		
25 °C; $I = 0.1$ M[15]	≈0	≈0	*b*	*b*
$[Pd(Et_4en)(H_2O)_2]^{2+}$	860 ± 25[c]	9.73 ± 0.02[c]	245 ± 4[e]	12.4 ± 0.04[e]
25 °C; $I = 0.1$ M[15]	≈0	≈0	1.29 ± 0.05	≈0
$[Pd(pic)(H_2O)_2]^{2+}$	7100 ± 300		25 400 ± 200	
10 °C; $I = 0.5$ M; pH 3.5	58 ± 9	32 ± 2	≈0	7.3 ± 0.7

[a] Too fast to be measured. [b] No data available. [c] pH 4.0. [d] pH 4.2. [e] pH 4.7.

(Table 1) for the first and second substitutions (scheme 12) of H_2O by the purine bases amounts to ca. 4 log units by which the first substitution step is favored above the second step. This leads to a much smaller slope (k_{13}) with respect to the intercept (k_{-13}) for the second step as compared to the first step. Steric hindrance caused by the 1:1 complex most probably accounts for the lower k_{13} value. Furthermore, the absorbance change associated with the kinetic traces of the second step is only about 10% compared to that for the first step, making it more difficult to resolve the second step since the error becomes too large. Assignment of the fast exponential function to the first reaction step was accomplished on the basis of reacting a 1:1 mixture of $[Pd(pic)(H_2O)_2]^{2+}$ and the nucleophile with an excess of ino or 5′-IMP, since the first step was then not observed.

The discrepancy between the thermodynamically and kinetically determined equilibrium constants is ascribed to the different conditions under which they were measured. The large discrepancy between the kinetically determined value for 5′-IMP (from Table 6, $K_{12} = k_{12}/k_{-12} = 123$ M^{-1}) with the thermodynamically determined value ($\log K_7 = 10.8$ from Table 1), must be due to different conditions selected for the substitution processes.[20] The kinetics were performed in weakly acidic medium at pH 3.5, which allows only the N7 positions of the purine bases to function as coordination sites. The thermodynamically determined equilibrium constants were titrated in more basic media, allowing also the N1 positions to serve as potential binding sites. Furthermore, the kinetically determined equilibrium constants are apparent values that must be corrected for all acid−base equilibria in solution.

In comparison with complexes of the type $[Pd(R_4en)(H_2O)_2]^{2+}$,[15] $[Pd(pic)(H_2O)_2]^{2+}$ reacts much faster with ino (see Table 6); even at 10 °C, the rates for $[Pd(pic)(H_2O)_2]^{2+}$ are much larger than those for the $[Pd(R_4en)(H_2O)_2]^{2+}$ type complexes at 25 °C. With 5′-IMP, the reactions proceed more slowly than those with ino, which contrasts with the case reported for the $[Pd(R_4en)(H_2O)_2]^{2+}$ complexes. By way of comparison, reactions of 5′-IMP and ino with [Pd(pic)(CBDCA)] proved to be slow and involved a series of reaction steps. Although these reactions were not investigated in any further detail, they could be of significance in the actual application of CBDCA complexes in the treatment of cancer (see Conclusions).

X-ray Structure of [Pd(pic)(CBDCA)]·2H$_2$O. The structure of [Pd(pic)(CBDCA)]·2H_2O is shown in Figure 6, and some selected bond lengths and angles are given in Table 7. Growing crystals of [Pd(pic)(CBDCA)]·2H_2O from water resulted in only thin needles of poor quality after several efforts. The square-planar nonsymmetric coordination sphere consists of two carboxylates and two amines coordinated to Pd(II). The Pd−N2 bond has a length (aromatic N) of 1.989(12) Å in comparison to the Pd−N1 bond length of 2.024 (12)Å, which is similar to 2.020(7) Å, observed for $[Pd(NH_3)_2(CBDCA)]$.[12] Although there is an apparent difference in the Pd−N bond lenghts, the error limits are such that it makes any detailed discussion irrelevant. Due to formation of a five-membered chelate ring, the N1−Pd−N2 angle of 82.3(5)° is smaller than that observed for monocoordinated amines (95° for N−Pd−N in $[Pd(NH_3)_2$-(CBDCA)][12]). The pyridine moiety and the planar coordination sphere are nearly coplanar, as indicated by the O1−Pd−N2−C6 torsion angle of only 2.9°. The Pd−O distances are 1.994-(11) Å for Pd−O1 and 2.008(11) Å for Pd−O2 (*trans* to pyridine). The six-membered chelate ring formed by Pd and CBDCA exhibits a boat conformation with a O1−Pd−O2 angle of 92.3(5)°. A slightly distorted structure is observed for the cyclobutane ring. The C9−C11−C12−C10 torsion angle has a magnitude of −18.3°, which indicates a deviation from a planar structure.

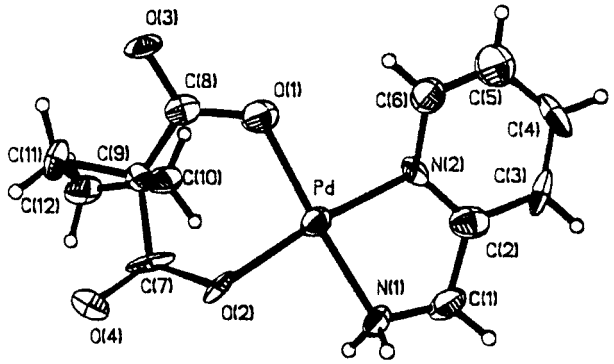

Figure 6. X-ray crystal structure of [Pd(pic)(CBDCA)]·2H_2O. The H_2O molecules are omitted for clarity.

Table 7. Selected Bond Lengths (Å) and Angles (deg) for [Pd(pic)(CBDCA)]·2H_2O

Pd−N1	2.024(0.012)	Pd−O1	1.994(0.011)
Pd−N2	1.989(0.012)	Pd−O2	2.008(0.011)
N1−Pd−N2	82.33(0.53)	Pd−N1−C1	112.72(0.98)
N1−Pd−O2	90.54(0.50)	Pd−N2−C2	114.73(1.07)
N2−Pd−O1	94.75(0.50)	Pd−N2−C6	124.01(1.19)
O1−Pd−O2	92.32(0.46)		

Conclusions

The introduction of a heteroaromatic nitrogen base into the Pd(II) coordination sphere results in an increase in acidity of the coordinated water molecules and a higher stability of complexes formed with nucleic base adducts. This is due to the π-accepting properties of pyridine decreasing the electron density on the metal center, thus making it more electrophilic.

In spite of oxygen donors being weaker ligands for Pd(II) than nitrogen- or sulfur-donor ligands, the bidentate CBDCA ligand shows a high affinity for the metal center and forms a stable complex that cannot be hydrolyzed at neutral pH. This

is of importance, especially when biological pH values and the high concentration of sulfur-containing amino acids or other potential ligands in the human blood are taken into consideration.

The 5′-monophosphate adducts of the purine bases show a higher stability than inosine itself, which can be related to stronger Coulombic forces between the di- or trinegatively charged monophosphate adduct and the positively charged metal complex. The 2-picolylamine also has an exocyclic NH_2 group that can be involved in hydrogen bonding with the phosphate, leading to an increase in stability of 5′-IMP and 5′-GMP over inosine. The reactivity of $[Pd(pic)(H_2O)_2]^{2+}$ toward ino is much larger than that for comparable $[Pd(R_4en)(H_2O)_2]^{2+}$ complexes, whereas for 5′-IMP it is about the same. The kinetic data clearly show that inosine is more reactive toward $[Pd(pic)(H_2O)_2]^{2+}$ than 5′-IMP, which can be attributed to a primary process that involves preassociation with the phosphate group in the case of 5′-IMP.

We conclude that the unique combination of the 2-picolylamine and CBDCA chelate ligands on the square-planar Pd(II) center exhibits promising properties for the further development of antitumor drugs. On the one hand, the CBDCA ligand exhibits exceptional stability toward hydrolysis reactions, whereas on the other hand the 2-picolylamine chelate introduces an important electronic tuning property. The extreme stability of the CBDCA complex in terms of stability constant and inertness to aquation suggests that the complex itself will be the reactive species in binding to DNA in the cell. Thus nucleophilic attack by DNA components on the CBDCA complex should represent the major reaction path, in contrast to the role of aquated species during such binding processes for other metal complexes.[7] Furthermore, the 2-picolylamine chelating ligand also introduces the possibility of effective intercalation into DNA, an aspect that could be of significance for the actual activity of this complex. Further modifications of the coodination sphere are presently underway, and it is our goal to develop a series of potential antitumor complexes of varying reactivity that can be employed for different types of tumors treated in different ways through the systematic tuning of spectator ligands.

Acknowledgments. The authors gratefully acknowledge the Deutsche Forschungsgemeinschaft, the Fonds der Chemischen Industrie, and the Volkswagen-Stiftung for financial support and the DAAD for a stipend to Mohamed Shoukry. We also thank Dr. G. Liehr for the collection of X-ray data and the solution of the structure.

Supporting Information Available: Listings of bond lengths and angles, atomic coordinates and equivalent isotropic displacement parameters, and anisotropic displacement parameters, stereoscopic pairs of perspective drawings and unit cell diagrams, and calculated species distribution plots and kinetic diagrams (16 pages). Ordering information is given on any current masthead page.

IC961192V